Research Square

Preprints are preliminary reports that have not undergone peer review.
They should not be considered conclusive, used to inform clinical practice,
or referenced by the media as validated information.

Urban green space and its co-evolution with socio-economic development in 10,511 global cities

Kunshu Yang
The University of Queensland
Yongping Wei
yongping.wei@uq.edu.au

The University of Queensland

Article

Keywords:

Posted Date: November 20th, 2026

DOI: https://doi.org/10.21203/rs.3.rs-10040555/v1

License: This work is licensed under a Creative Commons Attribution 4.0 International License.
Read Full License

Additional Declarations: No competing interests reported.

Urban green space and its co-evolution with socio-economic development in 10,511 global cities

Kunshu Yang[1], YongpingWei[1*]

[1] School of the Environment, the University of Queensland, Brisbane, QLD, Australia

∗ Author to whom any correspondence should be addressed.

E-mail: yongping.wei@uq.edu.au (Y. Wei)

Abstract

Urban development is increasingly expected to be both green and equitable. Yet urban green space (UGS), a central component of urban greenness, is rarely assessed as a multidimensional spatial structure or examined through its co-evolution with socio-economic development. Using 10,511 cities from the GHS-UCDB, we construct a multidimensional UGS index from 30-m land-cover data, use nighttime light intensity as socio-economic proxy, and analyse cities' co-evolutionary positions, green-prioritized rankings, transition pathways and structural correlates. We find persistent inequalities between North America/Europe and Africa/parts of Asia. Q1 cities with above-average relative greenness and socio-economic development generally dominated the green-prioritised ranking, but this status did not guarantee balanced co-evolution with nearly one-third of Q1 cities fell outside the top quartile. Factors associated with co-evolutionary position do not necessarily move cities toward more balanced green–socioeconomic development with clear regionality. These findings call for region-specific strategies to align greenness with socio-economic development.

Introduction

Development is no longer understood solely in terms of industrialization, infrastructure expansion, and economic growth, but increasingly considered as a green and equitable way. This shift is especially consequential for global cities, which already accommodate more than half of the global population and are projected to host 68% of the world's population by 2050 (Ramaswami et al., 2016; Zhang et al., 2022). Urban green space (UGS), including parks, urban forests, gardens, and green corridors, contributes to climate adaptation, heat mitigation, biodiversity conservation, recreation, public health, and urban liveability, making it a central component of urban greeness (Wolch et al., 2014; Li et al., 2023; McPhearson et al., 2021). However, it is a socially produced and spatially configured impacted by urban socio-economic development (Derkzen et al., 2017; Wilkerson et al., 2018; Wu et al., 2019; Zhang et al., 2022). Understanding how UGS is distributed, structured, and developed alongside socio-economic transformation is therefore foundational to assessing whether cities can pursue greener and more equitable development pathways.

Our previous study addressed several limitations in UGS inequality research by developing a relative UGS inequality index for more than 10,000 cities (Yang et al., 2026). It moved beyond absolute UGS measures by evaluating each city's green development against a common global average, thereby improving cross-city comparability. It also replaced the conventional Global North–South division with a continent–development–climate classification, enabling UGS inequality to be

interpreted across more specific urban contexts, and identified heterogeneous socio-economic, geographical, and climatic determinants across global city groups. However, the analysis mainly captured relative inequality patterns in quantity and did not account for the difference of internal structure of UGS. Consequently, global UGS inequality remains insufficiently understood as a multidimensional spatial structure (Zhang, 2023; Yang et al., 2021; Luo et al., 2025).

Cities have long been conceptualized as complex evolutionary systems shaped by nonlinear interactions and path-dependent dynamics (Allen, 1997). From this perspective, UGS and socio-economic development are two distinct but interacting pathways of urban transformation, with possible interaction dynamics including mutual reinforcement, lagged adjustment, and persistent mismatch over time (Alberti et al., 2017; Des Roches et al., 2021; McPhearson et al., 2021). Existing studies have provided important but fragmented evidence of environmental–socioeconomic interactions in cities, including the luxury effect in urban greenness, urban heat islands, the Environmental Kuznets Curve, air pollution–development decoupling, and carbon balance (Sulemana et al., 2017; Leong et al., 2018; Anguelovski et al., 2022; Böhringer et al., 2022; Yin et al., 2023; Behrer and Heft-Neal, 2024). However, it remains unclear how cities are positioned within the green–socioeconomic co-evolutionary relationship, how this relationship changes, and what structural conditions shape greener and more balanced trajectories.

To address these gaps, this study develops a green-prioritized co-evolutionary framework to examine how urban greenness and socio-economic development interact across global cities. Using 10,511 cities from the Global Human Settlement Layer Urban Centre Database (GHS-UCDB), we construct a multidimensional UGS index from global 30-m land-cover data. The index captures three aspects of urban green development: quantity, measured by patch number and mean patch size; compositional type, represented by grassland and forest–shrubland; and spatial organization, measured by aggregation and dispersion metrics. We use city-level nighttime light intensity as a globally comparable proxy for socio-economic development. Both UGS and nighttime light are transformed into relative indicators by centering each city against the annual global average, producing relative green development (UGSrel) and relative socio-economic development (NTLrel). We then construct a two-dimensional co-evolutionary space to classify cities into four relative positions based on whether UGSrel and NTLrel are above or below annual global averages. To evaluate balance between the two pathways, we apply signed-log transformation and pooled z-score standardisation before calculating balance distance and green-prioritised ranking. This allows us to distinguish high–high positional advantage from within-quadrant differences in balance and relative greenness. To capture temporal dynamics, we trace cross-quadrant transitions from 1990 to 2020 and decompose changes in UGSrel and NTLrel into synergy and mismatch axes. Finally, position and transition models identify the structural correlates of cities' co-evolutionary positions and interaction dynamics. Together, these steps assess how urban greenness and socio-economic development co-evolve globally, whether greenness keeps pace with socio-economic growth, and under what conditions greener and more balanced pathways may emerge.This will assist in developing global urban strategies for green and equitable development.

Results

North America had the highest mean UGSrel whereas Africa lowest being broadly stable over time

The UGSrel level in 2020 reveals a clear cross-continental pattern (Figure 1a and 1b). North America had the highest mean UGSrel (0.72), whereas Africa had the lowest (-0.14). Europe also showed a leading position (0.45), with many cities falling within the global top decile. Asia had a positive UGSrel, but it overally remained close to the global average (0.05). Despite these advantages, North America, Europe, and Oceania exhibited relatively large interquartile ranges, indicating within-continent heterogeneity. Upper-tail outliers appeared across all continents but were especially substantial in Asia, mainly in India (25.3%), China (23.8%), Bangladesh (13.3%), and Indonesia (10.2%).

A decomposition of UGSrel (Supplementary Figure 4) further shows that greenness advantage is multidimensional and continent-specific. Grassland and forest/shrubland exhibited broadly consistent spatial patterns. Cities in the global top decile for patch count and aggregation index (AI), for both grassland and forest/shrubland, were concentrated mainly in North America, Europe, and Asia, especially India, East Asia, and Southeast Asia. By contrast, cities in the global top decile for mean patch size and IMDI were more frequently found in Asia and Africa, particularly India, eastern China, and Central Africa. Taken together, these results indicate that cities in India shows an overall advantage across all four dimensions.

The temporal evolution of UGSrel (Figure 1c) shows that the continental ordering remained broadly stable over time. Changes in mean UGSrel were generally gradual, whereas within-continent inequality varied across continents. North America maintained a persistent relative advantage, with its mean UGSrel increasing slightly from 0.70 in 1990 to 0.72 in 2020, while Africa remained consistently negative. Europe showed a steady upward shift, from 0.34 to 0.45. Oceania exhibited a step-like increase around 2000 and then remained broadly stable. Asia increased modestly while staying close to the global average, whereas South America drifted slightly downward from positive to negative values. Within-continent dispersion also differed across regions (Supplementary Figure 5a), with North America and Oceania remaining more heterogeneous, while Africa and South America showed more convergent UGSrel patterns over time.

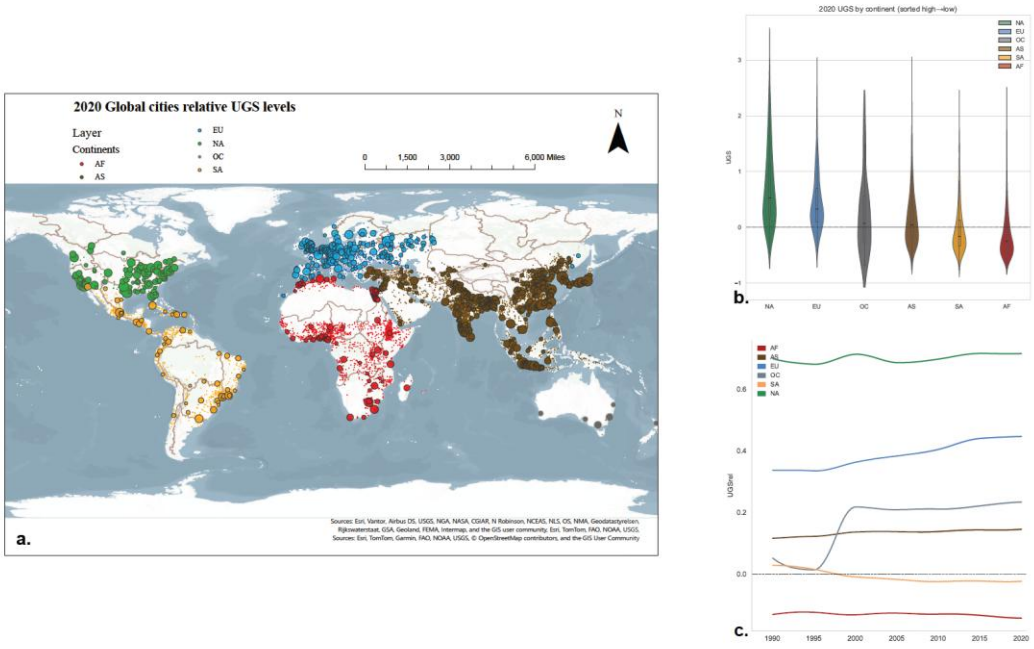


Figure 1 a. UGSrel distribution of global cities in 2020, green-North America, blue-Europe, brown-Asia, red-Africa, orange-South America, grey-Oceania; b. box-violin plots of UGSrel between continents; c. changes of median UGSrel values for continents from 1990 to 2020.

NTLrel was highest in North America while South America and Europe with marked increase during 2010-2015

The 2020 NTLrel (Figure 2a and 2b) distributions reveal a strong cross-continental hierarchy and geographic concentrated distribution, with developed regions having substantially higher NTLrel level than the developing regions. North America showed the highest level (median = 19.72, 113 cities fell into the global top decile), followed by South America, Europe, and Oceania. In contrast, Africa remained the lowest (mean = −0.22; median = −4.89). The advantage of North America was collective (low IQR), implying that the advantage was not driven by a small number of extreme cities. Europe and South America exhibited high levels but also stronger upper-tail (Europe 334.94; South America 222.77), such as cities from Russia, Spain, Italy and Netherlands of Europe, and cities from Mexico, Brazil, Argentina of South America. Asia and Africa showed low medians below the global average but "super-city" effects (long upper tails), for example, cities in the Middle East (e.g., Saudi Arabia, Qatar, and Turkey) and North Africa (e.g., Algeria, and Egypt).

Temporally, 2010–2015 marked a clear structural break where North America, South America and Europe simultaneous increased in their average NTLrel and within-continent dispersion (Figure 2c, and Supplementary Figure 5b), indicating a sharp widening of the internal development spread despite continued high-level cities. The change of NTLrel average in Africa and Asia was moderate, but their dispersion also expanded strongly and continued rising into 2020. Oceania showed comparatively stable dispersion and weak sensitivity to the 2015 shift.

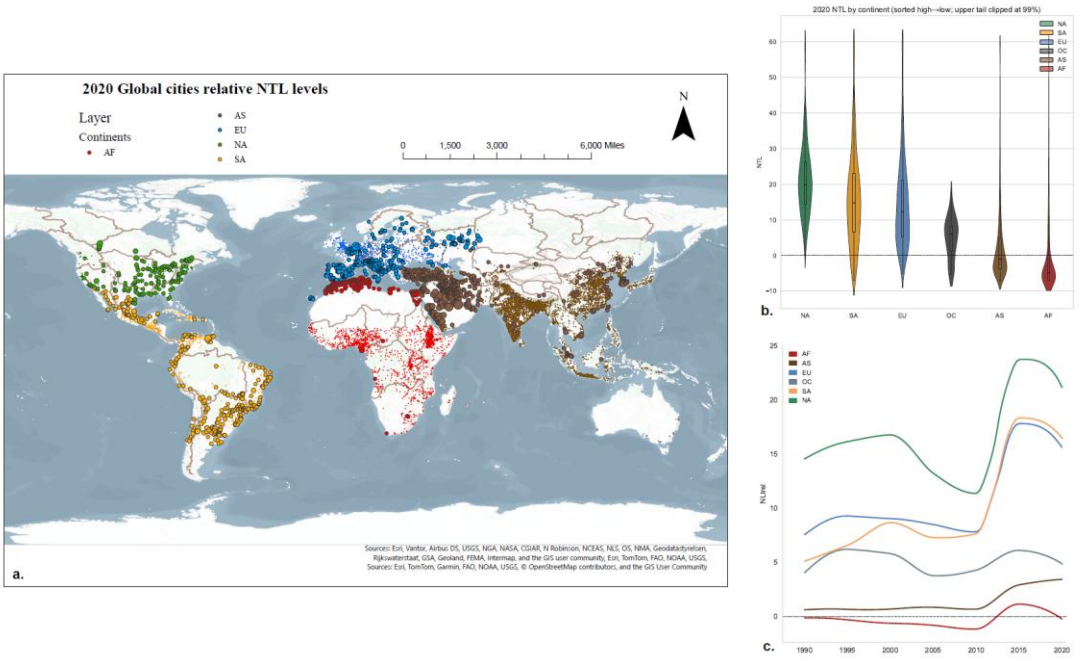


Figure 2 a. NTLrel distribution of global cities in 2020, green-North America, blue-Europe, brown-Asia, red-Africa, orange-South America, grey-Oceania; b. box-violin plots of NTLrel between continents; c. changes of median NTLrel values for continents from 1990 to 2020.

Cities with above-average greenness and socio-economic development do not necessarily indicate green-prioritized co-evolution while greenness-leading cities moved toward socio-economic catch-up

The 1990–2020 distribution of global cities in the UGSrel–NTLrel space revealed four co-evolutionary positions (Figure 3a). Q1 included 3,231 cities (29.2%),

concentrated in North America (269 of 305 cities, 88.2%) and Europe (747 of 968 cities, 77.2%), with large numbers also in China and India. Q3 was the largest quadrant, containing 3,567 cities (32.2%), mainly in Africa and Asia, especially India (1,099). In the mismatch quadrants, Q2 included 2,069 cities (18.7%), mainly from India (388), Brazil (210), and China (147), while Q4 included 2,195 cities (19.8%) and was dominated by Asian cities, especially China (604; e.g., Chengdu and Hangzhou) and India (560; e.g., Purnia and Gadag). After signed-log transformation and pooled z-score standardisation, the balance line indicated equality in standardised deviations between the greenness and socio-economic pathways. Under this scale-corrected interpretation, Q1 cities were not uniformly development-leading: 1,556 Q1 cities (48.2%) were above the standardised balance line, whereas 1,675 (51.8%) were below it. This indicates that high–high co-evolutionary status included substantial internal variation in the relative balance between greenness and socio-economic development.

The green-prioritised ranking in Figure 3b showed that high–high cities generally achieved stronger green-prioritised co-evolutionary performance after correcting the scale difference between UGSrel and NTLrel. Among the 3,231 Q1 cities, 2,285 (70.7%) were ranked in the city-level top 25%, while 946 (29.3%) did not enter the top quartile and 160 were ranked in the bottom 25%, such as in the United States (10), Italy (9) and Spain (8). The top quartile was therefore dominated by Q1 cities, which accounted for 82.6% of all top-ranked cities. However, the ranking also revealed important within-quadrant heterogeneity. The top quartile also included 330 Q3 cities (11.9%), 112 Q4 cities (4.1%), and 38 Q2 cities (1.4%). These Q3 cases should be interpreted as relatively balanced but low-level positions rather than fully desirable green-prioritised outcomes. By contrast, Q4 cities were no longer a major component of the top quartile under the scale-corrected ranking: only 112 Q4 cities (5.1% of all Q4 cities) entered the top quartile, while 854 Q4 cities (38.9%) were ranked in the bottom 25%. Overall, the ranking shows that Q1 generally represented the most favourable co-evolutionary position, but high–high status alone was still insufficient to guarantee top green-prioritised performance because balance and greenness strength varied substantially within Q1. Figure 3c identified 3,131 cities with cross-quadrant transitions between 1990 and 2020, accounting for 30.9% of the 10,143 cities with observations in both endpoint years. These movements were unevenly distributed across pathways. Vertical transitions accounted for 2,084 cities (66.6% of cross-quadrant transitions), exceeding horizontal transitions (757 cities, 24.2%) and diagonal transitions (290 cities, 9.3%). This indicates that changes in co-evolutionary position more frequently involved threshold-crossing in the socio-economic development dimension than in the greenness dimension or simultaneous movement across both dimensions. The largest transition pathway was Q4→Q1, involving 768 cities (24.5% of cross-quadrant transitions), indicating that many greenness-leading cities moved into the high–high quadrant through socio-economic catch-up. This pathway was concentrated in Asia, especially China, India, Vietnam, Turkey, and Indonesia, with examples including Ho Chi Minh City, Hanoi, Chengdu, and Hangzhou. Among Q1-related movements, 1,003 cities entered Q1, while 726 left Q1. By contrast, direct balanced upgrading from Q3→Q1 was rare, involving only 56 cities (1.8% of cross-quadrant transitions), and was concentrated mainly in Asia (43 cities), especially China (22) and India (17). Asia contributed 75.2% of all cross-quadrant transitions, mainly through Q4→Q1 and Q1→Q4 pathways.

Co-evolutionary improvement also occurred within stable quadrant positions (Supplementary Table 1). Among the 7,012 cities that remained in the same quadrant from 1990 to 2020, 1,676 showed simultaneous increases in both UGSrel and NTLrel. These included 1,035 Q1→Q1 cities, 477 Q2→Q2 cities, 104 Q3→Q3 cities, and 60 Q4→Q4 cities. These stable but improving cities were concentrated mainly in Asia (654) and Europe (515), especially India, China, Russia, Egypt, and the United States.

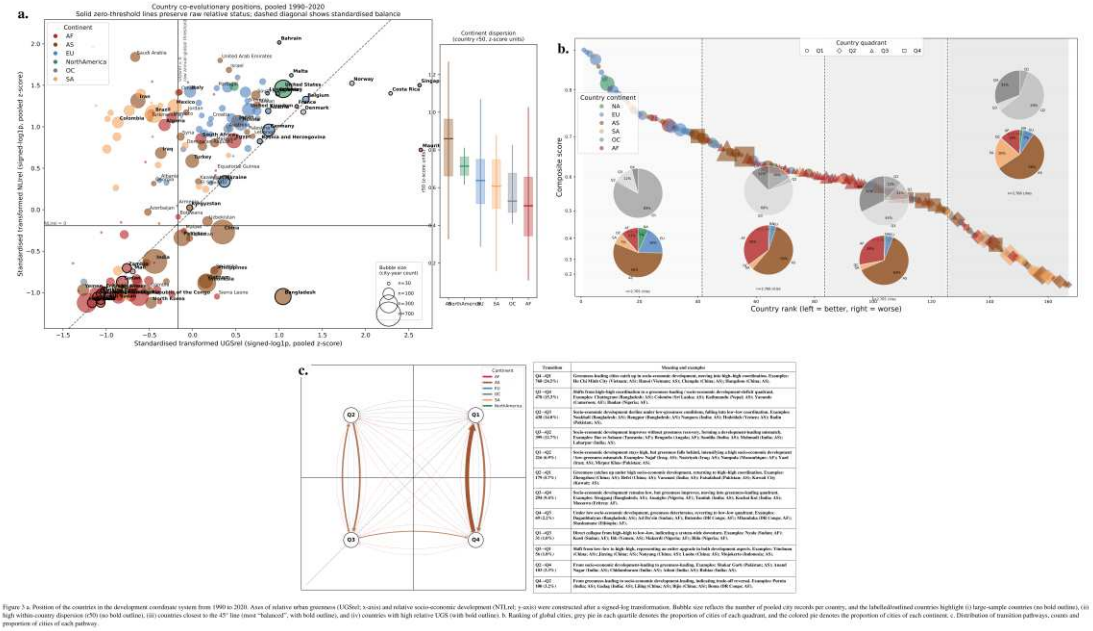


Figure 3 a. Position of the countries in the development coordinate system from 1990 to 2020. Axes of relative urban greenness (UGSrel; x-axis) and relative socio-economic development (NTLrel; y-axis) were constructed after a signed-log transformation. Bubble size reflects the number of pooled city records per country, and the labelled/outlined countries highlight (i) large-sample countries (no bold outline), (ii) high within-country dispersion (r50) (no bold outline), (iii) countries closest to the 45° line (most "balanced", with bold outline), and (iv) countries with high relative UGS (with bold outline). b. Ranking of global cities, grey pie in each quartile denotes the proportion of cities of each quadrant, and the colored pie denotes the proportion of cities of each continent. c. Transition pathways were classified using raw quadrant positions in 1990 and 2020. Arrow width indicates the number of cities in each transition pathway.

Pollution intensity and income shaped co-evolutionary positions while transition dynamics were structurally related to income and differentiated by regional biogeographic conditions

Position model shows that the two co-evolutionary pathways had different structural correlates. Globally, UGSrel was associated with a mixed set of socio-economic, climatic, and biogeographic factors. Pollution intensity showed the strongest positive association with UGSrel ($\beta^* = 0.301$), followed by income classes ($\beta^* = 0.228,\ 0.177,$ and 0.185 for income levels 2–4), whereas temperature showed the strongest negative association ($\beta^* = -0.203$). By contrast, NTLrel was mainly associated with socio-economic hierarchy, especially income level 4 ($\beta^* = 0.606$) and income level 3 ($\beta^* = 0.446$), while several climatic and biogeographic factors showed weaker or negative associations (Figure 4a).

At the continental level (Fig 4b, 4c), the dominant domains differed by pathway. For UGSrel, socio-economic factors (i.e., pollution intensity) dominated consistently across all six continents. For NTLrel, however, the dominant domains were more region-specific. Income level dominated in Asia and Europe. Biogeographic factors dominated in Africa, Oceania, and North America: biome types was the leading contributor in Africa and North America, while elevation level was the leading contributor in Oceania. South America showed a mixed socio-economic–biogeographic structure, with biome types ranking as the largest single contributor while income and GDP per capita also played important roles (Supplementary Fig. 7, Table 2).

Transition model further shows that the structural correlates of interaction dynamics differed from those of co-evolutionary position (Fig. 4d). Globally, higher income levels were positively associated with the co-evolutionary synergy axis S, especially income level 4 ($\theta_S = 1.270$), income level 3 ($\theta_S = 0.684$), and income level 2 ($\theta_S = 0.333$). However, higher income was also negatively associated with the co-evolutionary mismatch axis M, especially income level 4 ($\theta_M = -1.740$) and income level 3 ($\theta_M = -1.578$).

Continental patterns also differed between S and M (Fig 4e, 4f). For S, Asia was dominated by socio-economic-related factors, especially income. Africa showed a mixed biogeographic–climatic structure, with biome as the largest contributor. South America and Oceania were mainly associated with elevation level, while North America was mainly associated with catchment. Europe showed a weaker and more mixed structure, with pollution intensity ranking first but contributing only weakly to S. For M, Asia and Europe were more closely associated with socio-economic-related factors, especially income, with higher income levels indicating socio-economic-leading trajectories. By contrast, Africa, South America, and North America were dominated by biogeographic factors, particularly biome. Oceania showed weaker and less stable coefficient-level effects, with pollution intensity ranking highest (Supplementary Fig. 8, Table 3).

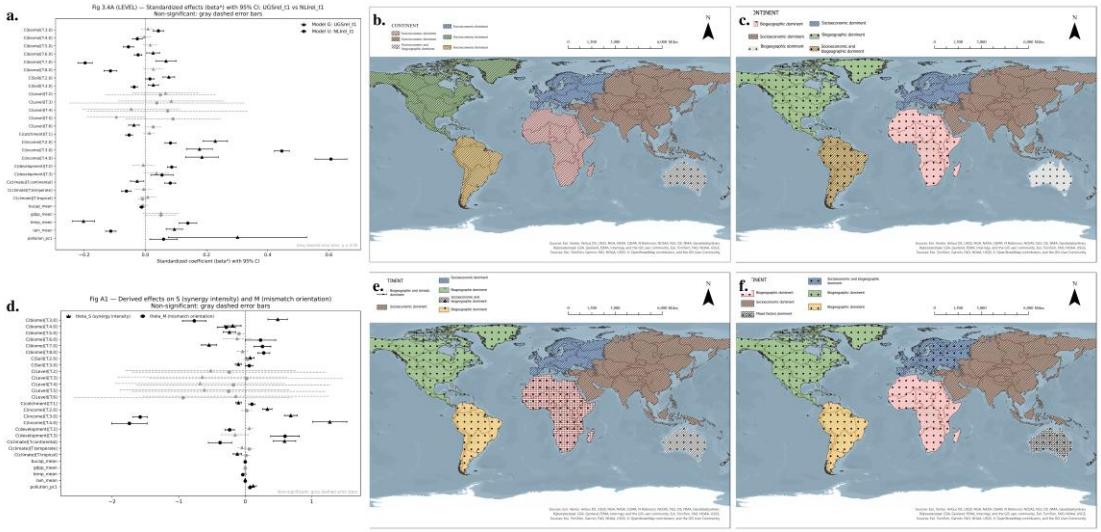


Figure 4 a. factors influencing the development position of global cities; b. dominant type of factors most associated with continental UGSrel; c. factors influencing continental NTLrel; d. factors influcening the development trajectories of global cities; e. main types of factors most associated with continental synergy development; f. main types of factors most associated with continental mismatch development.

Discussion

Our first finding shows that cities in well-developed regions generally occupied more advantageous positions in both UGSrel and NTLrel than those in less-developed regions, confirming pronounced global inequality in greenness and socio-economic development (Chen et al., 2022; Bille et al., 2023; Li et al., 2025). We extend this view by showing that the gap was not only large but persistent over the three decades since 1990, reflecting a cumulative and path-dependent process shaped by uneven development advantages, planning legacies, and differentiated ecological endowments (Young and McPherson, 2013; Anguelovski et al., 2022; Hölscher et al., 2023; Bakhtsiyarava et al., 2024). The decomposition of UGSrel further shows that regional differences were expressed not only in overall greenness but also in the structural forms of relative green advantage. In North America and Europe, higher UGSrel was more often associated with numerous and spatially aggregated green patches, consistent with institutionalized green-space planning and the long-term embedding of greening into redevelopment and governance (Chen et al., 2022; Young and McPherson, 2013; Hölscher et al., 2023). These larger green-space stocks, lower-density urban forms, and stronger planning traditions allow green areas to be protected as long-term urban assets. In parts of Asia and Africa, especially humid tropical or near-equatorial regions, relative green advantage was more strongly supported by ecological endowment and climatic suitability (Yan et al., 2021). However, their rapidly urbanising cities face the opportunity cost increase of maintaining green land (Enu et al., 2026). Therefore, the persistence of UGSrel inequality is not only a matter of ecological endowment, but also a result of uneven capacity to protect, finance, and institutionalise green space under development pressure. Cities with persistently low UGSrel may face greater difficulty keeping greenness aligned with future socio-economic growth. The long-term persistence of the UGSrel hierarchy therefore indicates that global green-space inequality is reproduced through cumulative advantage: historically greener and institutionally stronger cities are better able to maintain or upgrade their green-space systems, while cities under rapid urbanisation face stronger pressure to convert green land into built-up uses.

Our second finding shows that high–high co-evolutionary status generally represents a favourable position for green-prioritised development, Q1 cities dominated the top quartile of the green-prioritised ranking, indicating that cities with above-average greenness and socio-economic development were more likely to combine relatively strong green performance with balance between the two pathways. But it should not be interpreted as uniformly optimal. The top-ranked cities had their socio-economic development substantially outpaced relative greenness, meaning that their high–high status masked a development-leading imbalance. In addition, nearly 30% of Q1 cities showed lower ranking. This reflects the trajectory of many mature urban systems, where industrialization, infrastructure expansion, and growth-led urbanization were established earlier, while greening agendas were institutionalized later under densification, redevelopment pressure, and saturated urban space (Haaland and van den Bosch, 2015; Stijnen et al., 2024; Elmqvist et al., 2019). Q3 cities require a more cautious interpretation. Nearly 11.9% of them were closer to the balance line, mostly small and medium cities in India and China. This low-level synchronization is not desirable co-evolution, but it suggests that these cities may have opportunities to pursue more balanced development rather than repeating the trajectory of mature cities (Ramaswami et al., 2016; Wolch et al., 2014). Transition analysis reinforces this

point. Vertical transitions accounted for 2,084 cities (66.6%), indicating that co-evolutionary shifts were more often structurally related to relative socio-economic change, especially the Q4→Q1 pathway (Haaland and van Den Bosch, 2015; Wu et al., 2019; Zhang et al., 2022). To achieve green-prioritized co-evolution, Q3 cities should avoid development-led lock-in pathways. In addition, greenness-leading cities (Q4) were not a major component of the top-ranked group; instead, many Q4 cities entered Q1 through socio-economic catch-up, especially in Asia. This suggests that the main significance of Q4 lies less in its current green-prioritised performance and more in its transition potential. For cities with relatively strong greenness but weaker socio-economic development, the key challenge is to avoid development pathways that erode existing green advantages during economic catch-up.

Our third finding shows that factors associated with co-evolutionary positions do not necessarily move cities toward more balanced green–socioeconomic development. The position model shows that UGSrel was consistently associated with socio-economic-development-related factors across continents, especially pollution intensity, suggesting that broad urban-industrial intensity may reflect fiscal, infrastructural, and planning capacity for developing green infrastructure (Derkzen et al., 2017; Wilkerson et al., 2018; Han et al., 2023). By contrast, NTLrel was more region-specific, implying regionally specific social–ecological–infrastructural systems (Ramaswami et al., 2016; Seto et al., 2017). The transition model adds that higher income was linked to stronger synergy but also to socio-economic-leading mismatch. Continentally, Asia showed the strongest consistency between position and dynamics, both mainly associated with socio-economic-related factors, especially income. Africa, South America, and North America showed clear and different position–dynamic mismatch, requiring region-specific strategies. Asia should convert socio-economic momentum into green catch-up by linking infrastructure expansion, redevelopment, and new urban districts to green-space provision, ecological connectivity, and heat adaptation (Bille et al., 2023; Wilkerson et al., 2018; Li et al., 2024). Africa requires biome- and climate-sensitive strategies emphasizing suitable vegetation, heat mitigation, flood regulation, and water-sensitive design (Keeler et al., 2019; Ramaswami et al., 2016). South America should manage urban expansion while protecting ecological assets (Bakhtsiyarava et al., 2024). North America, Europe, and Oceania should pursue place-based and water-sensitive strategies that improve liveability and adaptation while avoiding unsustainable water demand (Keeler et al., 2019).

This study developed a comparative framework for examining how urban green space and socio-economic development jointly shape the developmental positions and transition pathways of global cities. First, we built a multidimensional city-level UGS index based on quantity, compositional type, and spatial organization, moving beyond single-metric measures of urban green development (Li et al., 2023; Zhang, 2023; Luo et al., 2025). Second, we constructed an urban development coordinate system based on UGSrel and NTLrel, allowing urban greenness to be interpreted together with, rather than separately from, socio-economic development. Third, by tracing quadrant transitions and decomposing trajectories into synergy and mismatch, we extended the framework from static description to dynamic interpretation, making it possible to examine where cities are positioned in green-prioritized co-evolution, how they evolve, and under what structural conditions more balanced pathways may emerge across different urban contexts. Several limitations remain. First, due to data

unavailability, the study does not include social, political, and institutional factors such as governance quality, planning effectiveness, institutional capacity, and political priorities (Eakin et al., 2017). Second, explanatory variables were treated as long-term contextual conditions rather than temporally matched causal drivers; the results should therefore be interpreted as structural associations rather than direct causal effects. Third, the analysis relies on broad continental comparisons. More refined typologies, such as urban hierarchy, climatic regime, or development stage, may reveal more specific development modes and intervention needs (Li et al., 2024).

Conclusion

This study develops a green-prioritized co-evolutionary framework to assess how urban green space (UGS) and socio-economic development jointly evolve across 10,511 global cities. By combining a multidimensional UGS index with a relative NTL index, we examined both cities' co-evolutionary positions and interaction dynamics. We found that, first, persistent inequality in co-evolutionary positions: cities in North America and Europe were more likely to occupy high–high positions, while many cities in Africa and parts of Asia remained in low–low positions. Second, high–high cities dominated the green-prioritised ranking, but high–high status was not sufficient to guarantee top performance because substantial within-quadrant differences remained in balance and greenness strength, while 24.5% greenness-leading cities achieved stronger green-prioritized co-evolutionary performance through relative socio-economic catch-up. Third, factors associated with co-evolutionary position do not necessarily move cities toward more balanced green–socioeconomic development. These findings will assist in developing global urban strategies for green and equitable development.

Methods

City sample selection and study period

The global urban samples were derived from the Global Human Settlement Layer Urban Centre Database (GHS-UCDB) (Melchiorri, et al., 2024). GHS-UCDB is the first globally harmonized database of urban centers. It provides a detailed and quantitative representation of land surface cover at a spatial resolution of 30 arc-seconds (approximately 1 km). GHS-UCDB offers a global depiction of sub-pixel urban cover fractions with year nodes of 1990, 2000, and 2015, including geographic attributes, socio-economic factors, environmental conditions, sustainable development goals, and disaster risk reduction metrics. The UGS was extracted from the "GLC_FCS30D Global 30-meter Land Cover Change Dataset (1985-2022)" (GLC_FCS30D) (Zhang et al., 2024), and the nighttime light was from the Global nighttime light dataset 1992 to 2022 (Tang et al., 2025). We selected 1990, 1995, 2000, 2005, 2010, 2015, and 2020 as the main comparative years to capture both long-term change and recent development dynamics while maintaining consistency across the UGS and NTL datasets. After matching city boundaries with complete UGS and NTL, 10,511 cities were retained for analysis. Cities were grouped by continent: North America (NA), Europe (EU), Oceania (OC), South America (SA), Asia (AS), and Africa (AF), to compare broad regional differences in co-evolutionary positions, trajectories, and structural correlates across global urban systems.

Definition and measurement of UGS equality index as the integrated greenness indicator of city development

We constructed a multidimensional UGS index to represent the urban greenness pathway in the green–socioeconomic co-evolution framework. To ensure global comparability and avoid the limitations of single-metric greenness measures, the index captured three dimensions of UGS: quantity, compositional type, and spatial organization (Supplementary Figure 1) (Li et al., 2023; Yang et al., 2021; Zhang, 2023; Luo et al., 2025).

Quantity was measured by patch count and mean patch size, representing the number and average size of green-space units within each city. Compositional type distinguished between grassland and forest–shrubland, reflecting differences in ecosystem-service potential across vegetation types (Keeler et al., 2019). Spatial organization was measured using the Aggregation Index (AI) and the Clark–Evans nearest-neighbour index (IMDI), capturing whether green-space patches were spatially aggregated or dispersed (Clark and Evans, 1954; McGarigal, 1995; He et al., 2000). These dimensions were integrated into a single UGS index to represent each city's relative green-development position in the co-evolutionary analysis.

The city-level UGS indicators were derived from the GLC_FCS30D. This dataset provides 35 land-cover subcategories across 26 time steps from 1985 to 2022, updated every five years before 2000 and annually thereafter (Zhang et al., 2024). All preprocessing and indicator extraction were conducted in Google Earth Engine (GEE). We reclassified the original land-cover categories into two broad vegetation groups. The first group was defined as herbaceous/productive green land, combining cropland and grassland. This aggregation was used because, in global 30 m land-cover products, cropland and grassland are both herbaceous vegetation types and may show similar spectral and seasonal characteristics, especially in peri-urban and urban–rural transition zones (Lu et al., 2010). Although cropland and grassland differ in land-use function, their separation is subject to classification uncertainty (73.04% in the

GLC_FCS30D) across heterogeneous climatic regions, agricultural systems, and vegetation phenologies. Aggregating them into a broader herbaceous/productive green category (grassland) therefore reduces the influence of fine-class classification noise in global cross-city comparison. The second group was defined as forest–shrubland, combining forest and shrubland classes. Together, these two groups represent major vegetation-covered land components within urban-centre boundaries, but should be interpreted as land-cover-based urban greenness rather than a direct measure of publicly accessible urban green space. These two classes represent the major green-space forms used to construct the urban greenness pathway in this study.

Green-space patches were identified in GEE based on pixel contiguity. To remove very small and potentially unstable fragments and improve cross-city comparability, only patches of at least 2 ha were retained (Martins, 2022). Using GHS-UCDB city boundaries, we extracted patch count and mean patch size separately for grassland and forest–shrubland in each city. Based on the identified patches and their spatial coordinates, we then calculated AI and IMDI for each city and each green-space class in Python.

$$AI = \frac{A_{obs}}{A_{max}} \times 100$$

$$A_{obs} = \frac{1}{2}\sum_i \sum_j a_{ij} \ , \ A_{max} = \frac{n(n-1)}{2}$$

Where a_{ij} is binary adjacency indicator for patch pair i, j, A_{obs} is the observed number of adjacent patch pairs, and A_{max} is the maximum possible number of patch pairs. Higher AI values indicate stronger aggregation and lower fragmentation of patches.

$$IMDI = \frac{r_{obs}}{E_{(r)}}$$

where r_{obs} is the observed mean nearest-neighbor distance between green-space patches, and $E_{(r)}$ is the expected mean nearest-neighbor distance under complete spatial randomness. The detailed formulation and statistical derivation of AI and IMDI are provided in the Supplementary.

Accordingly, the final city-level UGS indicator system comprised eight variables: grassland patch count, grassland mean patch size, forest–shrubland patch count, forest–shrubland mean patch size, grassland AI, forest–shrubland AI, grassland IMDI, and forest–shrubland IMDI. These indicators jointly capture the quantity, compositional quality, and spatial distribution characteristics of urban green spaces, and were subsequently used to construct the comparative UGS index for global cities. To integrate quantity, vegetation type, and spatial organisation into a single UGS index, we constructed a configuration-adjusted effective greenness measure. This formulation follows the landscape-ecology premise that green-space functions are shaped not only by the amount of vegetation but also by how vegetation patches are spatially organised. Landscape metrics such as aggregation and nearest-neighbour distance are widely used to represent landscape configuration, while urban green-space studies show that patch size, aggregation, fragmentation, and spatial distribution can influence ecosystem-service delivery, especially cooling and habitat-related functions. In this formulation, AI and IMDI were rescaled to [0, 1] and used as bounded exponents to represent how spatial organization modifies the contribution of green-space area to effective urban greenness. Grassland and forest–shrubland were

weighted using a pairwise comparison matrix based on their relative ecosystem-service potential (Keeler et al., 2019). The final UGS index was calculated as the weighted sum of grassland and forest–shrubland scores:

$$UGSIndex_t = \sum_k w_k \left(\mathrm{AreaTerm}_{k,t}\right)^{p_{k,t}}$$

where k denotes grassland and forest–shrubland, $\mathrm{AreaTerm}_{k,t}$ is the normalized and log-transformed total green space area, w_g (0.3333) and w_f (0.6667) are the normalized weights for grassland and forest–shrubland, and $p_{k,t}$ is a bounded exponent determined by AI and IMDI. To examine whether the construction of UGSrel was sensitive to the vegetation-type weights, we recalculated the UGS index using alternative weighting schemes for grassland and forest–shrubland. The baseline specification assigned a weight of 0.3333 to grassland and 0.6667 to forest–shrubland, reflecting the higher ecological importance of forest–shrubland in the configuration-adjusted UGS index (see details in supplementary Table 4 & 5).

To overcome the drawbacks of absolute UGS changes (Anguelovski et al., 2022; Yang et al., 2026), we applied the relative UGS index for each city at the global scale to represent the green city development level. The relative UGS equality index for each city was defined as:

$$UGSIndex_{trel} = UGSIndex_t - UGSIndex_{tglobal}$$

Measurement of urban nighttime light (NTL) equality as the socio-economic indicator of city development

City-level nighttime light intensity (NTL) was used to represent the socio-economic development pathway in the green–socioeconomic co-evolution framework. NTL provides a spatially continuous and globally comparable proxy for human activity, infrastructure intensity, and development concentration, and is particularly suitable for cross-city analyses where conventional socio-economic statistics are inconsistent in availability, scale, and comparability across countries (Gibson et al., 2021). We used the Global Nighttime Light Dataset from 1992 to 2022, which provides annual observations with digital number (DN) values ranging from 0 to 63 at a spatial resolution of 30 arc-seconds (Tang et al., 2025). This dataset improves the representation of low-light areas and enhances long-term cross-sensor consistency across the DMSP-OLS and VIIRS eras. All NTL processing was conducted in Google Earth Engine (GEE). For each comparative year, city polygons were overlaid with the annual NTL raster, and the mean DN value was extracted for each city to represent its overall socio-economic development intensity. We then calculated the relative NTL index to enable comparison across cities and years.

$$NTLIndex_{trel} = NTLIndex_t - NTLIndex_{tglobal}$$

Ranking global cities based on their integrative greenness ($UGSIndex_{trel}$) and socio-economic development ($NTLIndex_{trel}$)

To characterize the relative position of cities in the green–development co-evolutionary process, we constructed a two-dimensional co-evolutionary framework based on relative urban greenness (UGSrel) and relative nighttime light intensity (NTLrel) (Supplementary Figure 2). UGSrel was assigned to the horizontal axis to represent the urban greenness pathway, while NTLrel was assigned to the vertical axis to represent the socio-economic development pathway. Both indicators were centred

on the annual global average, so that positive values indicate above-average performance and negative values indicate below-average performance relative to all global cities in the same year.

We used the raw annual relative indicators to define cities' co-evolutionary positions. Using zero as the threshold for each dimension, cities were classified into four quadrants: Q1: UGSrel > 0 and NTLrel > 0; Q2: UGSrel < 0 and NTLrel > 0; Q3: UGSrel < 0 and NTLrel < 0; and Q4: UGSrel > 0 and NTLrel < 0. Q1 represents a high–high co-evolutionary position, where both greenness and socio-economic development are above the global average. Q3 represents a low–low co-evolutionary position, where both dimensions are below the global average. Q2 and Q4 represent two forms of asymmetric mismatch: Q2 indicates a socio-economic-development-leading mismatch, whereas Q4 indicates a greenness-leading mismatch. This quadrant classification was based only on the signs of the raw relative indicators, thereby preserving the interpretation of each quadrant as above or below the annual global average.

Because UGSrel and NTLrel have different numerical ranges and distributional properties, we did not use the raw line $UGSrel = NTLrel$ to evaluate balance. Instead, before calculating balance distance, green-prioritised ranking, and trajectory metrics, both variables were transformed using a signed-log function and then standardised into pooled z-scores (please find details in the Supplementary method). This transformation reduces the influence of extreme values and places the two pathways on a common scale. In the standardised co-evolutionary space, the balance line is defined as:

$$Y = X$$

This line represents equality in standardised deviations between the two pathways, rather than equality in their raw numerical values. Cities closer to this line were interpreted as having a more balanced relationship between the two development pathways, whereas cities farther from the line were interpreted as having stronger imbalance. This distinction allowed us to evaluate not only whether cities had relative advantages or disadvantages in the two dimensions, but also whether urban greenness kept pace with socio-economic development. The same co-evolutionary space was also used to trace changes in city positions over time and to distinguish whether trajectories moved toward synergy or mismatch.

For the green-prioritised ranking, each city was summarised by the median of its standardised coordinates across the study period:

$$X_i = \mathrm{median}_t(X_{it})$$
$$Y_i = \mathrm{median}_t(Y_{it})$$

The balance distance of city $i$was defined as its perpendicular distance from the standardised balance line:

$$D_i = \frac{|\, Y_i - X_i \,|}{\sqrt{2}}$$

A balance score was then obtained by reversing the min–max normalised distance:

$$Balance_i = 1 - \frac{D_i - \min(D)}{\max(D) - \min(D)}$$

Thus, cities closer to the standardised balance line received higher balance scores. To reflect the green-prioritised principle of this study, a second component was introduced to reward cities with stronger relative greenness. The standardised greenness coordinate was normalised to obtain the UGS score:

$$UGSScore_i = \frac{X_i - \min(X)}{\max(X) - \min(X)}$$

The final composite score was calculated as a weighted sum of the balance score and the UGS score:

$Composite_i = \omega_b Balance_i + \omega_u UGSScore_i$ where ω_b and ω_c denote the weight. To assess whether the green-prioritised ranking was sensitive to the selected weighting scheme, we recalculated the composite score using alternative balance–UGS weights ranging from 0.4/0.6 to 0.9/0.1 (supplementary Table 6). The main pattern was stable within the plausible range of 0.5/0.5 to 0.7/0.3: Q1 cities remained the dominant group in the top quartile, while Q4 cities contributed only a small share. When the balance weight was increased to 0.8 or above, however, Q3 cities entered the top quartile in large numbers, indicating that excessive emphasis on balance may over-reward low-level synchronisation. We therefore retained 0.6/0.4 as the main specification because it prioritises balance while still requiring a sufficiently strong greenness position. Cities were then ranked in a descending order of the $Composite_i$, such that higher-ranked cities were those that combined stronger balance between green and socio-economic development with a relatively higher UGS position.

Finally, to interpret cross-quadrant changes in the urban development processes from 1990 to 2020, we classified all possible transition pathways between the four quadrants into six paired groups: $Q1 \leftrightarrow Q4$, $Q2 \leftrightarrow Q3$, $Q1 \leftrightarrow Q2$, $Q3 \leftrightarrow Q4$, $Q1 \leftrightarrow Q3$, and $Q2 \leftrightarrow Q4$, their implications please see Table 1.

Table 1 Transition pathways and their implications

Group	Direction	Transition implications
Q1↔Q4	Q1→Q4 (NTL crosses below 0 while UGS remains ≥0)	Shifts from high–high coordination to a greenness-leading / socio-economic development-deficit quadrant.
	Q4→Q1 (NTL crosses above 0 while UGS remains ≥0)	Greenness-leading cities catch up in socio-economic development, moving into high–high coordination.
Q2↔Q3	Q2→Q3 (NTL crosses below 0 while UGS stays <0)	Socio-economic development falls to low-greenness conditions, transitioning into low–low coordination.
	Q3→Q2	Socio-economic development improves without greenness recovery, forming a development-leading mismatch.

	(NTL crosses above 0 while UGS remains <0)	
Q1↔Q2	Q1→Q2 (UGS crosses below 0 while NTL remains ≥0)	Socio-economic development stays high, but greenness falls behind, intensifying a high socio-economic development/low-greenness mismatch.
	Q2→Q1 (UGS crosses above 0 while NTL remains ≥0)	Greenness catches up into high socio-economic development, returning to high–high coordination.
Q3↔Q4	Q3→Q4 (UGS crosses above 0 while NTL stays <0)	Socio-economic development remains low, but greenness improves, moving into greenness-leading quadrant.
	Q4→Q3 (UGS crosses below 0 while NTL stays <0)	Greenness of cities under low socio-economic development deteriorates, reverting to low–low quadrant.
Q1↔Q3	Q1→Q3 (UGS and NTL both cross below 0)	Cities directly collapse from high–high to low–low, indicating a system-wide downturn.
	Q3→Q1 (UGS and NTL both cross above 0)	Cities shift from low–low to high–high, representing an entire upgrade in both development aspects.
Q2↔Q4	Q2→Q4 (Dimensional rotation (UGS↑, NTL↓)	Cities shift from socio-economic development-leading to greenness-leading.
	Q4→Q2 Dimensional rotation (UGS↓, NTL↑):	Cities shift from greenness-leading to socio-economic development-leading.

Determining geographical, socio-economical and climate factors of the development position of cities and their development trajectories

To move beyond descriptive mapping of city positions and their transition pathways, we conducted further analysis to identify the geographical, socio-economical and climate factors of the development position of cities and their develoment trajectories.

Model 1 for the development position of cities

We fitted two parallel linear models for NTLrel and UGSrel to identify the structural correlates of cities' green–development co-evolutionary positions. Because the co-evolutionary space is defined by two development pathways, the first model examined the socio-economic development pathway and the second examined the urban greenness pathway:

$$NTLrel_{i,t} = \alpha_U + X_{i,t}\beta_U + \delta_t + \nu_{i,t}$$
$$UGSrel_{i,t} = \alpha_G + X_{i,t}\beta_G + \delta_t + \epsilon_{i,t}$$

where i denotes city, $t$denotes year, X_i denotes the vector of long-term structural and contextual explanatory variables, and δ_t denotes period fixed effects that account for broad temporal shocks shared by all cities. The two equations were estimated separately but with the same predictors, allowing us to compare whether the structural correlates associated with the socio-economic development pathway were consistent with, or different from, those associated with the urban greenness pathway.

Model 2 for urban development trajectory

To identify the structural correlates of co-evolutionary interaction dynamics, we derived two dynamic response variables from changes in the two pathways of the co-evolutionary space. Specifically, the change in each relative dimension was calculated as the difference between two consecutive periods:

$$\Delta UGSrel_{i,t} = UGSrel_{i,t} - UGSrel_{i,t-1}$$
$$\Delta NTLrel_{i,t} = NLIrel_{i,t} - NLIrel_{i,t-1}$$

where $\Delta UGSrel_{i,t}$ and $\Delta NTLrel_{i,t}$ represent the direction and magnitude of change in a city's relative urban greenness and socio-economic development positions between adjacent periods.

The two change variables were then robustly standardized as $x$and y, where x represents standardized change in UGSrel and $y$represents standardized change in NTLrel. We then rotated the two-dimensional change space into two orthogonal axes:

$$S_\Delta = \frac{x+y}{\sqrt{2}}, \qquad M_\Delta = \frac{x-y}{\sqrt{2}}$$

where S_Δ represents the co-evolutionary synergy axis, capturing whether urban greenness and socio-economic development move jointly in the same direction. Positive S_Δ values indicate joint improvement in both pathways, whereas negative values indicate joint decline. M_Δ represents the co-evolutionary mismatch axis, capturing whether the trajectory is tilted toward relatively stronger greenness change or relatively stronger socio-economic change (Supplementary Figure 3). Positive M_Δ values indicate a greenness-leading trajectory, whereas negative values indicate a socio-economic development-leading trajectory. We then fitted a joint linear system using the same explanatory variables and period fixed effects as in Model 1 to identify the structural correlates of these interaction dynamics.

The explanatory variables X_i were derived primarily from the GHS-UCDB database and were selected to ensure broad sample coverage under a globally consistent framework. Because these covariates were available for only a limited number of years, they could not be matched to the full annual variation in UGSrel and NTLrel. We therefore treated them as long-term contextual conditions rather than short-term time-varying drivers. For continuous variables, we calculated city-level means over 1990–2015 and used them as time-invariant structural covariates. This approach follows the panel-data logic of using unit-specific means to capture between-city structural differences while allowing the outcome variables to retain temporal variation (Mundlak, 1978; Chatelain and Ralf, 2021). The explanatory variables included two groups. The first group comprised time-invariant categorical conditions, including biome, soil, elevation level, catchment, income class, development level, and climate type, which were treated as categorical predictors. The second group

comprised long-term mean covariates, including built-up area per capita ($bucap_mean$), GDP per capita ($gdpp_mean$), temperature ($temp_mean$), precipitation ($rain_mean$), PM2.5 emissions (pm_mean), and CO_2 emissions (c_mean). Because PM2.5 and CO_2 emissions represent related aspects of pollution intensity and may introduce collinearity, we combined them into a pollution intensity index using principal component analysis (PCA) (Roberts and Martin, 2006; Zhu et al., 2024). These variables were used to examine which structural conditions were associated with cities' co-evolutionary positions and interaction dynamics, rather than to estimate direct causal effects. After standardizing both variables, the first principal component was extracted as:

$$Pollution_i \equiv PC1_i = w_1 z(pm_mean_i) + w_2 z(c_mean_i)$$

The final variables were then grouped into three broad domains including socio-economic, climatic, and biogeographical variables (Table 2). The regression was therefore intended to identify which long-run structural and contextual characteristics of the cities were associated with their development distribution and development dynamics, rather than to estimate the causal effects.

Table 2 Summary of Explanatory variables

Domains	**Explanatory variables**	**Abbreviation**	**Definition**
Socio-economic (-related)	GDP per capita	gdpp_mean	The economic development level
	Built-up area per person	bucap_mean	Surface of the built-up area per person
	Pollution intensity index	pollution_pc1	Total emission of pollutants, reflecting the industrializing intensity.
	Development level	development	United Nations' urban development level
	Income Class	income	Inter-city income inequality
Climatic	Precipitation	rain_mean	Average precipitation for epoch
	Temperature	temp_mean	Average temperature for epoch
Biogeographic	Average elevation	Level	Average elevation of urban area
	Soil groups	Soil	Types and fertility of soil
	River basin	catchment	Number of major river basin(s)
	Biome	biome	Biome type(s)
	Climate types	climate	Four major climate classes

To interpret the relative importance of explanatory variables, we conducted a leave-one-out R^2-contribution analysis. For each outcome, we first estimated the full model and recorded its R^2. We then re-estimated the model after removing one explanatory variable at a time. The contribution of variable i was calculated as:

$$\Delta R_i^2 = R_{\text{full}}^2 - R_{-i}^2$$

where R_{-i}^2 is the R^2 of the reduced model after removing group i. A larger ΔR_i^2 indicates a stronger contribution to model explanatory power. We also calculated the relative contribution share and reported the overall direction of association for each ranked factor:

$$Share_i = \frac{\Delta R_i^2}{R_{\text{full}}^2}$$

Finally, we repeated the analysis separately by continent to compare whether the structural correlates of co-evolutionary positions and interaction dynamics differed across continental contexts.

First, all position and transition models were re-estimated using country-clustered standard errors. This adjustment accounts for non-independence among cities located within the same country, which may share institutional systems, planning traditions, national development conditions, and common measurement errors in globally harmonized datasets. Second, we estimated an alternative hierarchical robustness specification by adding continent fixed effects while retaining country-clustered standard errors. This specification accounts for broad continental baseline differences while still allowing within-country residual correlation. The position models used UGSrel and NTLrel as dependent variables and included year fixed effects. The transition models used the co-evolutionary synergy axis, ΔS, and the co-evolutionary mismatch axis, ΔM, as dependent variables and included transition-period fixed effects. The purpose of these checks was not to estimate causal effects, but to evaluate whether the main structural associations were robust to continent-level heterogeneity (please find robustness results in the supplementary table 7).

Acknowledgements
This work was supported by the University of Queensland Graduate School for Research Training Program scholarship and the Australian Research Council project (Project ID: DP220103054).

Data availability
The data that support the findings of this study are openly available at the following URL/DOI: https://github.com/KunshuY/urban-study.git

Conflict of interest
The authors declare that they have no known competing financial interests or personal relationships that could have appeared to influence the work reported in this paper.

Author Contribution
Kunshu Yang designed the study, wrote the main manuscript text and prepared all figures and tables. Yongping Wei designed the study, reviewed and revised the manuscript.

References
Alberti, M., Marzluff, J., & Hunt, V. M. (2017). Urban driven phenotypic changes: empirical observations and theoretical implications for eco-evolutionary feedback. *Philosophical Transactions of the Royal Society B: Biological Sciences*, 372(1712).
Allen, P. M. (1997). Cities and regions as evolutionary, complex systems. *Geographical Systems,* 4, 103-130.

Anguelovski, I., Connolly, J. J., Cole, H., Garcia-Lamarca, M., Triguero-Mas, M., Baró, F., ... & Minaya, J. M. (2022). Green gentrification in European and North American cities. *Nature Communications*, *13*(1), 3816.
Bakhtsiyarava, M., Moran, M., Ju, Y., Zhou, Y., Rodriguez, D. A., Dronova, I., ... & Skaba, D. A. (2024). Potential drivers of urban green space availability in Latin American cities. *Nature Cities*, *1*(12), 842-852.
Behrer, A. P., & Heft-Neal, S. (2024). Higher air pollution in wealthy districts of most low-and middle-income countries. *Nature Sustainability*, *7*(2), 203-212.
Bille, R. A., Jensen, K. E., & Buitenwerf, R. (2023). Global patterns in urban green space are strongly linked to human development and population density. *Urban Forestry & Urban Greening*, *86*, 127980.
Böhringer, C., Fischer, C., Rosendahl, K. E., & Rutherford, T. F. (2022). Potential impacts and challenges of border carbon adjustments. *Nature Climate Change*, *12*(1), 22-29.
Chatelain, J. B., & Ralf, K. (2021). Inference on time-invariant variables using panel data: A pretest estimator. *Economic Modelling*, *97*, 157-166.
Chen, B., Wu, S., Song, Y., Webster, C., Xu, B., & Gong, P. (2022). Contrasting inequality in human exposure to greenspace between cities of Global North and Global South. *Nature Communications*, *13*(1), 4636.
Clark, P. J., & Evans, F. C. (1954). Distance to nearest neighbor as a measure of spatial relationships in populations. *Ecology*, *35*(4), 445-453.
Derkzen, M. L., van Teeffelen, A. J., Nagendra, H., & Verburg, P. H. (2017). Shifting roles of urban green space in the context of urban development and global change. *Current Opinion in Environmental Sustainability*, 29, 32-39.
Des Roches, S., Brans, K. I., Lambert, M. R., Rivkin, L. R., Savage, A. M., Schell, C. J., ... & Alberti, M. (2021). Socio-eco-evolutionary dynamics in cities. *Evolutionary Applications*, *14*(1), 248-267.
Eakin, H., Bojórquez-Tapia, L. A., Janssen, M. A., Georgescu, M., Manuel-Navarrete, D., Vivoni, E. R., ... & Lerner, A. M. (2017). Urban resilience efforts must consider social and political forces. *Proceedings of the National Academy of Sciences*, *114*(2), 186-189.
Elmqvist, T., Andersson, E., Frantzeskaki, N., McPhearson, T., Olsson, P., Gaffney, O., ... & Folke, C. (2019). Sustainability and resilience for transformation in the urban century. *Nature Sustainability*, *2*(4), 267-273.
Enu, K.B., Zingraff-Hamed, A., Lupp, G. *et al.* (2026). Overcoming barriers to micro-scale greening in rapidly urbanizing Sub-Saharan African cities: empirical insights from Ghana. *npj Urban Sustain*, *6*, 58. Gibson, J., Olivia, S., Boe-Gibson, G., & Li, C. (2021). Which night lights data should we use in economics, and where?. *Journal of Development Economics*, *149*, 102602.
Haaland, C., & van Den Bosch, C. K. (2015). Challenges and strategies for urban green-space planning in cities undergoing densification: A review. *Urban Forestry & Urban Greening*, *14*(4), 760-771.
Han, Y., He, J., Liu, D., Zhao, H., & Huang, J. (2023). Inequality in urban green provision: A comparative study of large cities throughout the world. *Sustainable Cities and Society*, *89*, 104229.
He, H. S., DeZonia, B. E., & Mladenoff, D. J. (2000). An aggregation index (AI) to quantify spatial patterns of landscapes. *Landscape ecology*, *15*(7), 591-601.
Hölscher, K., Frantzeskaki, N., Collier, M. J., Connop, S., Kooijman, E. D., Lodder, M., ... & Vos, P. (2023). Strategies for mainstreaming nature-based solutions in urban governance capacities in ten European cities. *npj Urban Sustainability*, *3*(1), 54.

Keeler, B. L., Hamel, P., McPhearson, T., Hamann, M. H., Donahue, M. L., Meza Prado, K. A., ... & Wood, S. A. (2019). Social-ecological and technological factors moderate the value of urban nature. *Nature Sustainability*, *2*(1), 29-38.
Leong, M., Dunn, R. R., & Trautwein, M. D. (2018). Biodiversity and socio-economics in the city: a review of the luxury effect. *Biology letters*, *14*(5).
Li, W., Wei, Y., Chen, L., Chen, Z., Li, M., Chen, W., ... & Zhao, Q. (2025). Multiple environmental inequalities between Global South and Global North in over 10,000 urban centers. *npj Urban Sustainability*.
Li, Y., Ren, C., Ho, J. Y. E., & Shi, Y. (2023). Landscape metrics in assessing how the configuration of urban green spaces affects their cooling effect: A systematic review of empirical studies. *Landscape and Urban Planning*, *239*, 104842.
Li, Y., Svenning, J. C., Zhou, W., Zhu, K., Abrams, J. F., Lenton, T. M., ... & Xu, C. (2024). Green spaces provide substantial but unequal urban cooling globally. *Nature Communications*, *15*(1), 7108.
Lu, D., Hetrick, S., & Moran, E. (2010). Land cover classification in a complex urban-rural landscape with QuickBird imagery. *Photogrammetric Engineering & Remote Sensing*, *76*(10), 1159-1168.
Luo, F., Zhang, Y., Kong, Z., & Dai, Y. (2025). Which green is more equitable? A multi-indicator urban green space assessment across vulnerable population groups from an environmental justice perspective. *Ecological Indicators*, *178*, 113948.
Luo, L., Wang, Y., Liu, Y., Zhang, X., & Fang, X. (2022). Where is the pathway to sustainable urban development? Coupling coordination evaluation and configuration analysis between low-carbon development and eco-environment: A case study of the Yellow River Basin, China. *Ecological Indicators*, *144*, 109473.
Martins, B. (2022). Where to construct new urban green spaces to be at the recommended distance from users and to complement existing ones? A study in five cities of northern Portugal. *Urban Forestry & Urban Greening*, *72*, 127571.
McGarigal, K. (1995). *FRAGSTATS: spatial pattern analysis program for quantifying landscape structure* (Vol. 351). US Department of Agriculture, Forest Service, Pacific Northwest Research Station.
McPhearson, T., M. Raymond, C., Gulsrud, N., Albert, C., Coles, N., Fagerholm, N., ... & Vierikko, K. (2021). Radical changes are needed for transformations to a good Anthropocene. *Npj Urban Sustainability*, *1*(1), 5.
Mundlak, Y. (1978). On the pooling of time series and cross section data. *Econometrica: Journal of the Econometric Society*, 69-85.
Opdam, P., Verboom, J., & Pouwels, R. (2003). Landscape cohesion: an index for the conservation potential of landscapes for biodiversity. *Landscape Ecology*, *18*(2), 113-126.
Przewoźna, P., Inglot, A., Mielewczyk, M., Maczka, K., & Matczak, P. (2024). Accessibility to urban green spaces: A critical review of WHO recommendations in the light of tree-covered areas assessment. *Ecological Indicators*, *166*, 112548.
Ramaswami, A., Russell, A. G., Culligan, P. J., Sharma, K. R., & Kumar, E. (2016). Meta-principles for developing smart, sustainable, and healthy cities. *Science*, *352*(6288), 940-943.
Roberts, S., & Martin, M. (2006). Using supervised principal components analysis to assess multiple pollutant effects. *Environ Health Perspect*. 114(12):1877-82.doi: 10.1289/ehp.9226.
Seto, K. C., Golden, J. S., Alberti, M., & Turner, B. L. (2017). Sustainability in an urbanizing planet. *Proceedings of the National Academy of Sciences*, *114* (34), 8935-8938.

Stijnen, C., Frantzeskaki, N., & Wijsman, K. (2024). Beating around the bush: A scoping review of trade-offs for just planning and governance of urban nature-based solutions. *Urban Forestry & Urban Greening*, *102*, 128525.
Sulemana, I., James, H. S., & Rikoon, J. S. (2017). Environmental Kuznets Curves for air pollution in African and developed countries: exploring turning point incomes and the role of democracy. *Journal of Environmental Economics and Policy*, *6*(2), 134-152.
Tang, H., Zhong, Y., Deng, J., Xia, H., & Wei, J. (2025). Global nighttime light dataset from 1992 to 2022 with focus on low-light areas. *Scientific Data*, *12*(1), 982.
Turner, M. G. (1989). Landscape ecology: the effect of pattern on process. *Annual Review of Ecology and Systematics*, 171-197.Wilkerson, M. L., Mitchell, M. G., Shanahan, D., Wilson, K. A., Ives, C. D., Lovelock, C. E., & Rhodes, J. R. (2018). The role of socio-economic factors in planning and managing urban ecosystem services. *Ecosystem Services*, *31*, 102-110.
Wolch, J. R., Byrne, J., & Newell, J. P. (2014). Urban green space, public health, and environmental justice: The challenge of making cities 'just green enough'. Landscape and Urban Planning, 125, 234-244.
Wu, S., Liang, Z., & Li, S. (2019). Relationships between urban development level and urban vegetation states: A global perspective. *Urban Forestry & Urban Greening*, *38*, 215-222.
Yan, Y., Mao, K., Shen, X., Cao, M., Xu, T., Guo, Z., & Bao, Q. (2021). Evaluation of the influence of ENSO on tropical vegetation in long time series using a new indicator. *Ecological Indicators*, *129*, 107872.
Yang, K., Wei, Y., Li, J., & Li, W. (2026). Urban green space inequality and its socio-economic, geographical, and climate determinants in 11 528 cities. *Environmental Research Letters*, *21*(1), 014008.
Yang, Z., Fang, C., Mu, X., Li, G., & Xu, G. (2021). Urban green space quality in China: Quality measurement, spatial heterogeneity pattern and influencing factor. *Urban Forestry & Urban Greening*, *66*, 127381
Yin, Y., He, L., Wennberg, P. O., & Frankenberg, C. (2023). Unequal exposure to heatwaves in Los Angeles: Impact of uneven green spaces. *Science Advances*, *9*(17), eade8501.
Young, R. F., & McPherson, E. G. (2013). Governing metropolitan green infrastructure in the United States. *Landscape and Urban Planning*, *109*(1), 67-75.
Zhang, F., Chung, C. K. L., & Yin, Z. (2020). Green infrastructure for China's new urbanisation: A case study of greenway development in Maanshan. *Urban Studies*, *57*(3), 508-524.
Zhang, J. (2023). Inequalities in the quality and proximity of green space exposure are more pronounced than in quantity aspect: Evidence from a rapidly urbanizing Chinese city. *Urban Forestry & Urban Greening*, *79*, 127811.
Zhang, L., Yang, L., Zohner, C. M., Crowther, T. W., Li, M., Shen, F., ... & Zhou, C. (2022). Direct and indirect impacts of urbanization on vegetation growth across the world's cities. *Science Advances*, *8*(27), eabo0095.
Zhang, X., Zhao, T., Xu, H., Liu, W., Wang, J., Chen, X., & Liu, L. (2024). GLC_FCS30D: the first global 30 m land-cover dynamics monitoring product with a fine classification system for the period from 1985 to 2022 generated using dense-time-series Landsat imagery and the continuous change-detection method. *Earth System Science Data*, *16*(3), 1353-1381.

Zhu, G., Wen, Y., Cao, K., He, S., & Wang, T. (2024). A review of common statistical methods for dealing with multiple pollutant mixtures and multiple exposures. *Frontiers in Public Health*, *12*, 1377685.

Supplementary Files

This is a list of supplementary files associated with this preprint. Click to download.

- Supplementary.docx